Optimizing Engineering Components of an Integrated Nucleic Acid Diagnostic Device for Pulmonary Tuberculosis

Connie Yu

Keck Graduate Institute
Niemz Research Lab
Summer Undergraduate Research Experience

June-August 2016

Abstract

Consisting of an electronic instrument and disposable cartridges, an integrated nucleic acid testing device to diagnose pulmonary tuberculosis at the point of care has been developed for use in low-resource setttings. Engineering progress on the cartridge focused on optimizing the amplification and detection of *Mycobacterium tuberculosis* (*M.Tb*) DNA from sputum, particularly in the components of the electrolysis-driven pumps, reaction insert for isothermal nucleic acid amplification, and lateral flow strip detection chamber. Confirmation that electrode material and electrolyte volume play significant roles in electrolytic pumping provided information for future methods to increase pump rate to target ranges. Several elements of the ePump assembly were also redesigned to address issues with venting and pump rates. Testing of the temperature difference between the instrument heater and the reaction chamber provided information on the pouch and fluid layers' influence on heating. Preliminary testing for optimal positions and depths of pressure bars to keep layers of the strip in contact has identified a few key positions for pressure, with progress to be done to finalize the pressure for each location. Together, these optimized components will help provide high disease burden areas with greater access to an inexpensive, fully automated diagnosis option for tuberculosis.

Introduction

With a death rate of nearly 50% in developing parts of the world, tuberculosis (TB) is the leading cause of death from infectious disease. This airborne bacterial infection generally attacks the patient's lungs, although it can spread to almost any other part of the body. Around a third of the world is infected with latent TB, meaning that they do not exhibit symptoms, but this dormancy can be disrupted with malnutrition, old age, or HIV infection [1].

Compared to diagnostic efforts, vaccines are a less feasible option to combat the spread of this disease due to the difficulty of creating a vaccination effective for the general population. Patients' reactions to current TB vaccines range so widely from case to case that even though the BCG vaccine against TB is one of the most widely administered vaccinations, it has only about 60% success in providing protection [2]. Current methods of diagnosing TB include the TB skin test and blood test, but these tests fail to differentiate latent TB infection from the fully developed disease. Other options that can differentiate the TB disease from latent infection such as sputum microscopy sacrifice speed for accuracy: while results can be obtained within hours, accuracy ranges from only 50-60%. Accuracy of such techniques can be increased, but with a tradeoff in cost of the expensive materials required [3]. The main high burden areas for TB are also low-resource settings, and these methods of diagnosis are not ideal for these environments where continuous power sources are scarce and disposable income for healthcare even more so.

Having a low-cost, portable diagnostic device for use in developing areas of the world at the point of care would leave fewer cases undetected and thus untreated. Addressing this need, the overarching goal of this project is to create an integrated nucleic acid testing device to diagnose pulmonary tuberculosis. This device, which consists of disposable cartridges and an electronic instrument for controlling fluidics and heating, will execute sample preparation, isothermal DNA amplification, and lateral flow based detection without any user intervention by analyzing the sputum of a possibly infected individual. The process begins with the injection of a sputum sample into the cartridge, and subsequent steps are automated once the cartridge is inserted into the instrument. Preprocessing for the sputum involves liquefaction and disinfection. The sample is then blended in an omnivalve containing microbeads that extract DNA from the cells. Wash buffer is pumped through to remove excess material, and elution buffer harvests the

DNA from the microbeads. This eluate is pumped to a reaction chamber where isothermal nucleic acid amplification occurs on top of a heating platform in the instrument. The amplified mastermix is then wicked onto a lateral flow strip for detection [4].

Feasibility studies of the alpha prototype have been conducted using spiked and clinical sputum samples. The device accurately detected disease in spiked samples with 10^5 and 10^4 colony forming units (CFU)/mL, though at 10^3 CFU/mL accuracy dropped to 73%. Clinical sputum samples were also tested with the device and compared to qPCR results, and with only one false positive and two false negatives, the alpha device demonstrated overall 90% sensitivity and 96% specificity, which are promising statistics for just a preliminary prototype. Progressing to the beta prototype, a more robust and manufacturable upgrade of the alpha version, engineering efforts have focused on optimizing hardware components for amplification and detection within the integrated cartridge, particularly three main parts: the electrolytic pumping (ePump) system for fluid movement, the reaction insert for isothermal amplification, and the

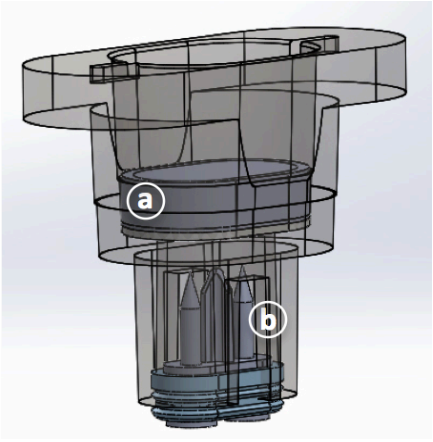

Figure 1: Isolated design of beta's ePump assembly featuring a) encapsulated electrolyte with b) two electrodes connected by a septum positioned underneath

lateral flow strip chamber for detection.

The ePump relies on electrolysis: electrical current runs through electrodes submerged in an electrolyte, which splits water molecules into hydrogen and oxygen gas that displace and thus pump fluid downstream. Figure 1 displays the basic assembly design in the beta prototype: liquid electrolyte is encapsulated to prevent evaporation and spillage, and the electrodes are housed

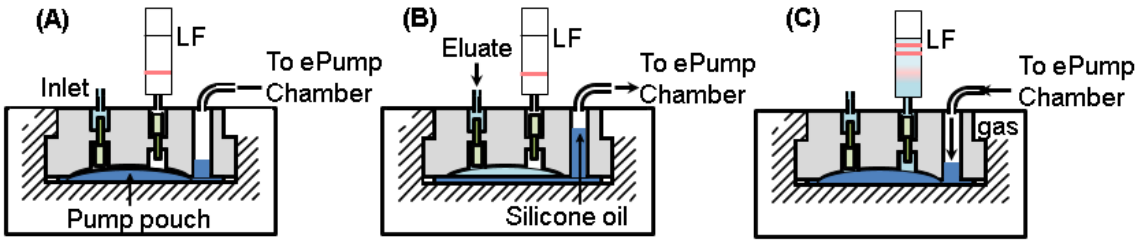

Figure 2: Operation of reaction insert for isothermal nucleic acid amplification

A) Prior to cartridge operation, silicone oil fills the pump pouch
B) After eluate enters reaction chamber, pump pouch is evacuated and reconstituted mastermix is heated for amplification
C) After reaction, ePump pushes silicone oil to fill pump pouch and eject amplified matter onto lateral flow strip for detection

below the capsule because they would corrode if left in electrolyte. Once the cartridge is inserted into the instrument, bosses below the cartridge push the electrodes up to puncture the bottom seal of the electrolyte capsules.

The reaction insert is the location of the duplex isothermal nucleic acid amplification for the internal control and the sputum's harvested DNA. It includes an elliptical reaction chamber for amplification, attachment bosses for fastening to the cartridge, check valves to prevent backflow, and a pump pouch for pumping amplified mastermix. Mastermix, dehydrated to ensure longevity, is sealed within the reaction chamber and a pump pouch is sealed on top of it. Figure 2 demonstrates the operation of the reaction insert. During cartridge and insert assembly, the pump pouch below the reaction chamber is filled with silicone oil. In the amplification portion of cartridge operation, eluate enters the reaction chamber, displacing the silicone oil. A heating platform heats the reconstituted mastermix for amplification, and afterward an ePump pushes silicone oil to fill the pump pouch and thus eject amplified mastermix for detection.

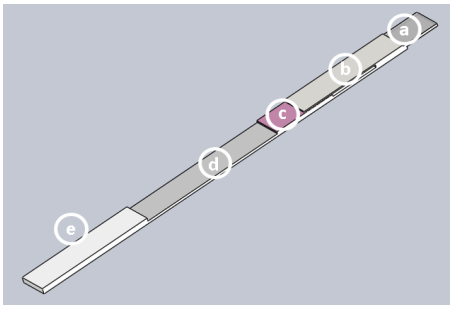

Figure 3: Layers of a lateral flow strip

A) Glass wick draws up fluid to the strip
B) Sample pad collects sample
C) Detection conjugates on conjugate pad bind to analyte
D) Immobilized antibodies or antigens on the nitrocellulose membrane bind to analyte and detection conjugates, forming visible stripes
E) Absorbent pad captures excess fluid and helps with capillary action

A lateral flow strip that lies downstream of the reaction chamber is used for analyzing the amplified mastermix. Its many layers, as shown in figure 3, interact with each other to detect analyte in the sample. A glass wick connected to the strip wicks the sample from the holding chamber and onto the strip. Detection begins when sample and buffer reaches the strip's sample pad. The conjugate pad below it houses detection conjugates that bind to any analyte present in the sample. Capillary action pulls the fluid mixture onto a nitrocellulose membrane where lines of immobilized antibodies or antigens bind to the target analyte and detection conjugate, causing stripes to appear. An absorbent pad at the end of the strip helps wick fluid down the strip and captures any excess buffer [4]. For proper development of the strip, these layers must remain in contact with one another as amplified mastermix wicks through the strip. The cartridge lid features pressure bars that press on the strip in the lateral flow chamber to ensure this.

Optimization of each cartridge feature focuses on proper thermal or fluidic control. The goal of ePump optimization focuses on obtaining a consistently reproducible pump rate ranging from 100µL/min to 1mL/min. This flow rate should be controllable by increasing or decreasing the voltage across the reaction's electrodes in order to have different pump rates for the different pumping steps of the cartridge system. Because the alpha system had flow rates lower than desirable, parameters of the electrolyte and electrode, such as electrolyte volume and electrode

material, were altered and tested to achieve the target ranges of pump rate. The major problematic factor of the ePump, however, relates to the venting of the electrolyte capsule. Electrodes easily puncture the capsule's bottom film, but the top seal must also be opened to allow the reaction-generated gas to escape. Because the thermally bonded seal currently consists of a layer of aluminum with two layers of different plastic on either side, this robust film is difficult to tear without creating an air-tight seal around the base of the puncturing object.

For the reaction insert, a major short term goal focused on proper temperature control: the instrument controls a thermistor-regulated heater for the isothermal amplification, but because layers of fluid and plastic lie between this heater and the reaction chamber, there is a finite difference in temperature between the instrument-controlled temperature and the final temperature that fluid in the reaction chamber reaches. This delta should be consistent to ensure uniform results, and the instrument should reliably account for this temperature difference when handling the heater's set point for complete amplification. To mass produce reaction inserts to test thermal control on the instrument testbed, an injection mold was designed with customizable layers to define different geometries on the top and bottom surfaces of the insert, since geometry is still in a flexible stage of development.

Optimization in the lateral flow strip chamber concentrated on testing different positions and depths of pressure bars that would press down from the lid and onto particular places on the strip. With these optimal pressure points in place, the lateral flow strip should develop with complete, even lines without streaking or visual ambiguity. For proper fluid handling, the pressure points should also prevent fluid from flowing over, under, or along the sides of the strip.

After the three components achieve the goals for proper fluidic and thermal control, manufacturability considerations must be factored in to make the cartridge inexpensive enough

for the targeted low-resources areas. Those modifications might find the optimized features too complex for production, necessitating future iterations to make the part more scalable. Even so, the progress will provide valuable insight on designing each component for proper operation.

Materials and Methods

Progress relied on the design and fabrication of prototypes and testbeds. SolidWorks was used to create computer-aided designs (CADs), which were then fabricated in house. Fabrication methods made use of 3D printing on the Dimension 1200es, CNC milling on the Rolland MDX-40, and injection molding on the Morgan Press. Other machining tools such as drill presses and band saws were used in conjunction with those main techniques.

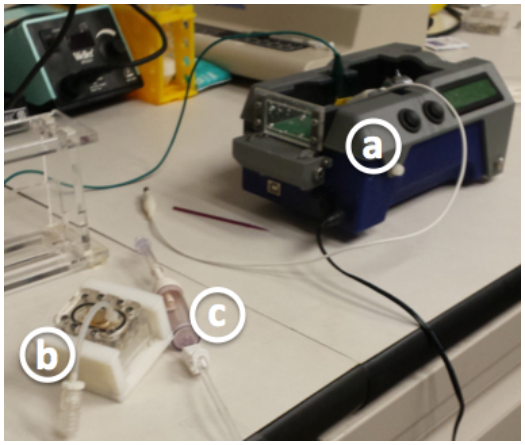

Figure 4: Assembly for ePump testing

A) Alpha instrument testbed
B) Isolated ePump testbed
C) Drip chamber and tubing for water displacement

In the optimization of the ePump, early efforts went toward testing different electrolyte and electrode parameters to achieve the target pumping range of 100µL/min to1mL/min. Pump testing was conducted using the assembly depicted in Figure 4 to confirm a linear relationship between electrode's exposed surface area to electrolyte versus flow rate. An isolated ePump testbed was attached to the alpha instrument testbed, which provided current for the electrodes. The electrodes used were the ones integrated in the alpha cartridge –1.26mm diameter stainless

steel, 3/8" long nails– and triplicates of trials used 120, 200, and 288μL of a 1M $NaSO_4$ electrolytic solution (6.41, 10.71, and 15.44 mm^2 in surface area, respectively). The ePump testbed lid was connected to tubing and a drip chamber to quantify gas production by recording the volume of displaced water. To ignore the issue of venting in capsules, electrolyte was directly pipetted into the ePump testbed's capsule chamber instead of encapsulation.

Different nail material and dimensions were also tested in the goal of exploring ways to vary and increase pump rate. 1/2" long, 1.26mm diameter steel and 0.5mm diameter nickel-plated stainless steel nails were substituted for the original electrodes in the alpha cartridge. The testing was conducted in triplicates and used the same isolated ePump and alpha instrument testbeds as in the flow rate versus surface area experiment. Because the nickel-plated nail had a thinner diameter, exposed surface area was kept constant for comparison to the control case of the original nail by increasing the electrolyte volume by a calculated factor of 2.4.

To create iterations in the ePump spike and capsule assembly, acrylonitrile-butadiene-styrene (ABS) was CNC milled or 3D printed. SolidWorks was used for modeling each upgraded design, which cycled through different positions and sizes of syringe-inspired protrusions. Each iteration's success was measured using the same testbeds and water displacement quantification as previously mentioned in other ePump experiments. To interface with the beta instrument testbed, an acrylic pseudo-cartridge was machined with one removable ePump chamber. To mass-produce capsules for tests, an injection mold with interchangeable inserts was designed

To test thermal control in reaction inserts using the beta testbed, the same pseudo-cartridge for the ePump was machined to include space for the reaction insert fastening. Rubber septa capped off the inlets and outlets leading to the reaction chamber and pump pouch, which were filled with water (to substitute eluate) and silicone oil, respectively. To track temperature

differences, thermocouples interfacing with TracerDAQ software were secured inside the reaction insert and on top of the heating platform. The thermocouple on the heater was later removed because it interfered with the insert-to-heater contact, and the instrument's temperature measurements were used instead. To minimize heat dissipation, insulation foam was cut and pressed on top of the reaction insert. Exchangeable inserts for the pseudo-cartridge were designed and machined in order to accommodate different fastening bosses on the reaction inserts, should the bosses' geometry change in the future. An injection mold was created for rapid production of simple inserts to be used in thermal control testing. These inserts, depicted in

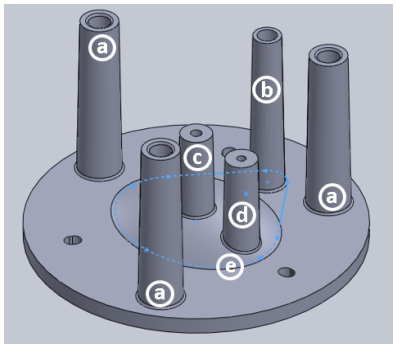

Figure 5: CAD of simplified reaction insert

A) Attachment bosses for fastening to cartridge
B) Silicone oil pump pouch inlet
C) Inlet to reaction chamber
D) Outlet to reaction chamber
E) Outline of teardrop seal for pump

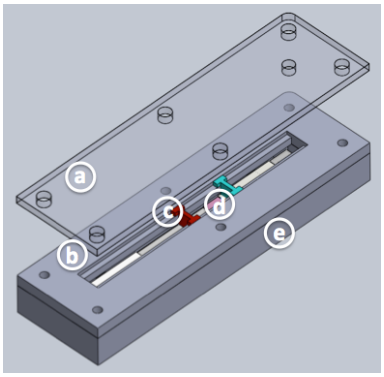

Figure 6: CAD of sliding lid testbed

A) Top layer for fastening
B) Slot for pressure point repositioning
C) Pressure bars color-coded with different depths
D) Lateral flow strip
E) Bottom chamber for strip

Figure 5, featured plain inlets and outlets for filling the reaction chamber and pump pouch, without considering the necessary geometry and locations for interfacing with other components of the cartridge. Once the pseudo-cartridge was fully assembled with the reaction insert and thermocouple in place, the beta heating platform was set to 63°C for one hour.

Shown in Figure 6, a sliding lid for testing different pressure points along the lateral flow strip was machined out of acrylic, and color-coded acrylic bars of different depths were milled using measurements obtained using a micrometer and calipers along a lateral flow strip. 10nM

concentrations of oligonucleotide surrogates for the amplicon and internal amplification control (IAC) were used for testing fluidic control, with elution buffer used to bring volume to 100-110uL. Time for the liquid to fully wick through the entire strip was recorded for comparison of the bars' influence on the speed and visibility of analyte detection development.

Results and Discussion

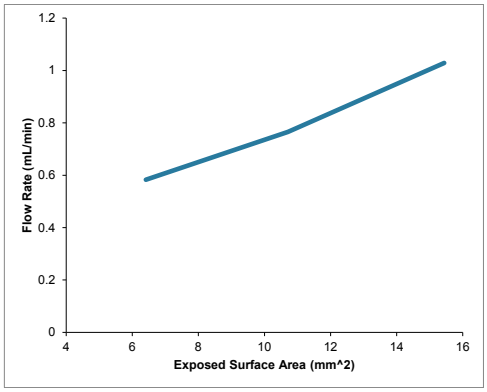

Figure 7: Plot of flow rate vs. exposed surface area

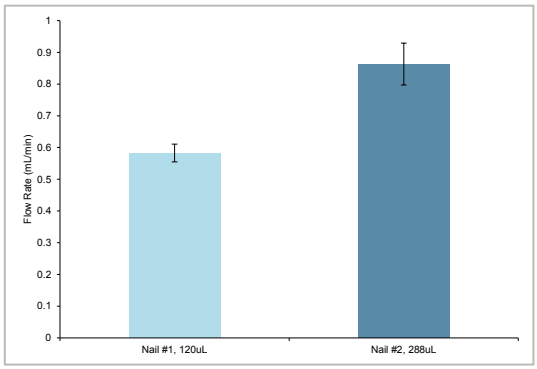

Figure 8: Comparison of flow rates from 1.26mm diameter stainless steel electrodes (nail #1) vs. 0.5mm nickel-plated stainless steel electrodes (nail #2)

Because electrolysis depends on the amount of the electrodes' surface area exposed to the electrolyte, increasing electrolyte volume should increase surface area exposed, thus increasing the ePump's overall pump rate. Figure 7 displays data of flow rate (in mL/min) versus electrode's exposed surface area (in mm^2). A linear regression line fits well along the connected data points, confirming this expectation of a linear relationship between the two. In the future, this relationship can be used to extrapolate the exposed surface area (and thus volume of electrolyte) required to achieve a particular pump rate, though the limitation on this would be the volume constraint of the capsule, especially if the capsule houses a spike for venting the top seal.

Different metals were hypothesized to have varying efficiencies in energizing water molecules for gas production, and the steel and nickel-plated electrode substitutions confirmed this. When the amount of surface area exposed was kept constant for each type of electrode, the nickel-plated stainless steel nails performed better than the plain stainless steel nail, the first

pumping 0.25mL more per minute than the latter, as reflected in Figure 8. Even the steel nails

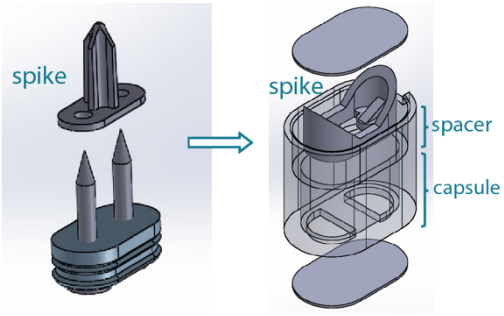

Figure 9: Comparison of original spike on top of electrode and septum assembly (left) to redesigned spike sealed within capsule (right)

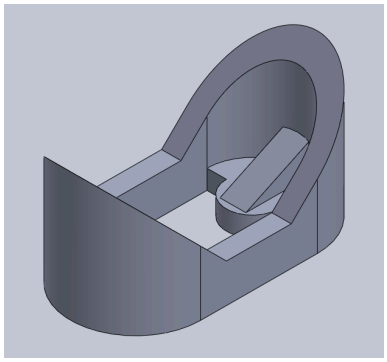

Figure 10: CAD of most successful spike iteration

without plating performed roughly 20% better than the original stainless steel ones. These results suggest that seeking alternative coating or base material options for the electrodes could be used for adjusting pump rate to desirable levels when the range is lower or higher than needed.

Original plans to vent the capsule involved a single protrusion machined as part of the shim that sits on top of the septum, as shown in the left CAD in Figure 9. However, the plastic in the thermally bonded film created an airtight barrier around the spike, preventing gas from venting out. To circumvent this issue, the redesigned spike, shown in the right CAD of Figure 9, sealed with the electrolyte inside a redesigned capsule for assembly. As the electrodes puncture the bottom of the capsule, the spike inside would pushed be upward to pierce the top seal.

Iterations of the spike used in capsule venting relied on compromising many factors. Sturdier spikes would be more stable for propping open the top seal, but they would also occupy more space that could otherwise be filled by electrolyte. Bigger protrusions would create larger airways for venting, but the larger radius of curvature would be more locally flat, allowing bunched up film to cover airways more easily. The final spike iteration, pictured in Figure 10, features two syringe-inspired protrusion whose outer walls are extended so the inner wall of the capsule can guide the spike upward. Platforms on the left and right side provide an interface for

the electrodes to easily align themselves before pushing up the spike, and the open gap in the middle of the spike allows for bubble formation to be easily vented upward. Even the capsule was redesigned for better integration of this spike: it features an extended guide wall (spacer) to keep the capsule in place against the lid and to prevent the spike from tilting as it travels upward past the top film. A rectangle was added to the middle of the capsule's bottom surface to prevent the nails from crossing and creating short circuits, and a notch at the top guides air to channels.

Rather than puncturing through the top seal as done by most iterations, this spike consistently disrupts the thermal bond, leaving only a one-point contact between the seal and capsule. The remaining issue with this spike is that the 3D printed version outperforms the machined one in consistency and pumping. Because 3D printing is not a scalable manufacturing process, the machined version must be comparable if not superior to the 3D printed one. The 3D printed version has a blunter, lower-resolution tip that may be more effective in peeling off the top film as opposed to cutting through it as the machined version does. The 3D printed version is also slightly smaller from shrinkage after printing, and this margin of tolerance from the

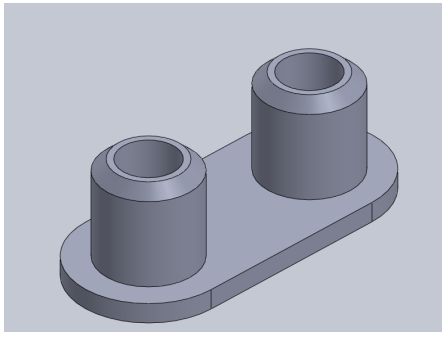

Figure 11: Redesigned shim for protecting electrodes

capsule's inner wall allows it to tilt once it reaches the top film and better lever it off.

While the seal can now be consistently broken, an initial delay in pumping persists. This was originally attributed to pressure buildup from the spike's inadequate puncturing of the top

film. Upon further experimentation, the aluminum layer of the capsule's bottom seal is believed to be the source of the hysteresis. The aluminum contact on the electrodes provides an alternative path for current instead of the electrolytic solution, and this short circuit delays the pumping until the aluminum becomes passivated. A redesigned shim, shown in Figure 11, was machined with sleeves that protect the electrodes and prevent this short circuit from occurring. Testing is in progress to determine optimal geometries, such as an adequate height for the protrusions without covering up too much of the electrodes. The degree and direction of chamfer might be altered to enhance the shim's success in protecting the electrodes. There was also interference with the capsule's bottom surface as the protrusions attempted to enter the capsule along with the electrodes, so the capsule may be changed to better accommodate the shim.

Temperature control tests demonstrated a delta of 2.2°C between the instrument heater and inside the reaction chamber. Reproducibility was an issue because each insert's reaction chamber and pump pouch must be filled with minimal bubbles, but some inserts could end up with more bubbles or less fluid. The interface between the heater and insert also proved to be difficult to control because the attachment bosses are too thin to provide a hard stop for fastening. This variability affected temperature readings, but once effort was put toward filling the pouches with consistent volumes of fluid, an average temperature of 61.8°C with a standard deviation of 0.31°C was measured inside the reaction chamber.

Preliminary testing on the sliding lid testbed for lateral flow detection revealed the lateral flow strip to be less sensitive to subtle changes in pressure as long as the pressure is present. The position of most pressure points have yet to be significantly changed for experimentation, but the pressure bar holding down the absorbent pad was moved to the far end, resulting in visibility improvements. A pressure point on the absorbent pad is necessary to prevent the strip from

bowing upward from the other pressure points, but it also blocks the negative pressure provided by the pad and thus prevents fluid from wicking farther into the strip. Moving this pressure point allows more fluid to travel down the strip and prevents excess that from building up around the sides of the chamber.

Conclusion

Testing of the alpha and beta ePump testbeds provided knowledge on the relationships between flow rate and electrode or electrolyte parameters. Substituting plating and base material alternatives to the current electrodes expanded future possibilities for adjusting pump rate into target ranges. A key consideration for the electrodes, however, is that the length is constrained to 3/8" due to the cartridge's height restrictions: the 1/2" long nails used in substitute testing would have to be sourced with the correct length.

After several prototypes for the ePump's spike and capsule, the top seal of the capsule was been successfully and consistently propped open with the redesigned assembly. Successes and failures revealed the importance of guiding features for the spike to avoid major tilting when traveling upward. Another key feature is the ability to rip open the top seal as opposed to puncturing it: disrupting the seal leaves a larger gap for airflow compared to the narrower airways provided by a punctured seal. The 3D printed version's consistency in outperforming its machined counterpart poses a problem for manufacturability. Future spike optimization will alter the machined version to be comparable if not better than the 3D printed counterpart, possibly by machining a blunter tip or slightly undersizing the spike to allow for some controlled tilting.

A redesigned shim is undergoing iterative prototyping to make the initial pump delay more reproducible, but even if it works reliably in the end, a holistic look at the ePump's complexity must be analyzed with regards to manufacturability. The redesigned spike and shim

system might succeed in producing robust ePumps, but the overall assembly may be too complicated for manufacturing at a low cost, and thus other options would need to be pursued. Even so, pinpointing key features of the shim and spike required for proper pumping will be important progress to be used in the future.

The protocol for temperature testing will need additional adjustments for less variation in experimental parameters. Additional iterations of the reaction insert will be designed to incorporate all the inlet/outlet bosses for the insert, and corresponding inserts will be milled to create these prototypes by in house injection molding. The topography of the reaction insert is still being optimized for proper fluid handling and temperature control, in addition to geometric considerations to avoid heat sinks in the injection mold manufacturing process. Future consideration will also be needed to determine the location and geometry of the venting barrier required for air displacement when eluate is pumped to the reaction chamber.

Testing on the sliding lid testbed for the lateral flow chamber showed that the lateral flow strip allows a wide tolerance to subtle changes in pressure depth, but more testing will further characterize this tolerance and analyze additional combinations of the pressure bar's location and depths. Another issue to be addressed in the future is venting in this chamber: because the liquid flows through the strip, it displaces air that needs to be vented out of the cartridge. Possibilities include a hydrophobic venting barrier that will let only air and not buffer out, similar to the venting barrier of the reaction chamber. Its geometry and location will need to be finalized and integrated onto a suitable position.

Even after these three subsections of the cartridge have been individually optimized, integration into a single system will need to check for possible interference among the components, especially as all three interact with one another. Feasibility does not necessitate

manufacturability, and ensuring that the overall device is inexpensive and scalable for production to targeted low resource settings will entail additional iterations in order to bring this technology to the point of care in homes around the world.

References

1. World Health Organization (2016) Tuberculosis. Retrieved August 11, 2016, from www.who.int/mediacentre/factsheets/fs104/en/
2. World Health Organization (2016) Biologicals: BCG Vaccine. Retrieved August 11, 2016, from www.who.int/biologicals/areas/vaccines/bcg/en/
3. Kanabus, Annabel (2016) Skin test, Sputum and Other Types of TB Test. Global Health Education. Retrieved August 11, 2016, from www.tbfacts.org
4. Roskos K, Hickerson AI, Lu H-W, Ferguson TM, Shinde DN, Klaue Y, et al. (2013) Simple System for Isothermal DNA Amplification Coupled to Lateral Flow Detection. PLoS ONE 8(7): e69355. doi:10.1371/journal.pone.0069355
5. Program for Appropriate Technology in Health (2016) Diagnostic Techniques: Lateral Flow Strips. Retrieved August 11, 2016, from www.sites.path.org/dx/rapid-dx/technologies/lateral-flow/
6. Laboratory Notebook, CYI

Appendix

Electrolytic hydrogels were explored as a possible improvement in the ePumps, and while hydrogel proved to be impracticable concept for the final ePump system, the experience revealed considerations that may be useful for future progress. Additionally, ePump testing was conducted on the beta instrument testbed in order to confirm and quantify the relationship between current running through the ePump and the resulting pump rate. This correlation will be useful for future progress on optimizing the controllability of the pump rate so that different rates can be accurately achieved for fluidic handling in the cartridge by changing the input current from the instrument.

Minor side experiments were also conducted to characterize the performance of various components in order to progress with the other goals for the major three cartridge components mentioned. This exploration includes data on pressure buildup in the ePump when the electrodes are pushed into the capsule, and even the relationship between electrolyte concentration and pump rate was considered. To access the relevant methods and results, please refer to reference #6.

Electrolytic Hydrogel

Additional research on the ePumps explored stabilization of the electrolyte by using an electrolytic hydrogel instead of the liquid electrolyte currently used. Because hydrogels are more

viscous than liquids, they could act as a more stable medium for gas bubbles to form and move upward for venting. The higher surface tension of the hydrogel would allow larger bubbles to grow and float upward to release gas through the top vent of the capsule, an improvement from the typical mini bubble and foam formation that pushes out the liquid electrolyte.

Protocols from previous research done on hydrogel formation were used as a beginning reference point. Hydroethyl cellulose (HEC) was the polymerization factor added to trisodium citrate solutions and stirred for 1-2 hours (depending on salt concentration) for hydrogel formation. Sodium sulfate was added to turn the hydrogel electrolytic for use in the ePump, and citric acid was used for pH adjustment when needed. The problem with getting the sodium sulfate into solution with the HEC and trisodium citrate came from the high concentration of sodium sulfate required to make the gel electrolytic. This is likely because the salt solvation monopolizes water molecules that would the hydrogel requires for complete polymerization. When the salt dissolves in the water, it monopolizes water molecules that would otherwise be used for hydrogel formation. Lowering the salt concentration frees up water molecules for proper hydrogel formation. Once the concentration of sodium sulfate was lowered from the original 1M as used in the liquid electrolyte to 0.75M and below, hydrogels could finally form.

The creation of an electrolytic hydrogel was made possible only by lowering the concentration of sodium sulfate added to the HEC and trisodium citrate. However, the cost of lowering salt concentration corresponded to a lower achievable pump rate. Adding to this handicap, the hydrogel's viscosity and higher surface tension increased foam formation instead of the larger bubbles that were expected, thus allowing the electrolyte to be more easily pumped out. Little to no gas was generated and pumped out by the electrolytic hydrogels due to this compounded issue, suggesting that an electrolytic hydrogel would worsen the bubbling issue that

it was intended to fix. Although the concept of the electrolytic hydrogel is not applicable for the final ePump system, the experience revealed the importance of even phase properties (electrolyte viscosity, in particular) for the ePump's performance.

Characterization of EPump Current's Effect on Flow Rate

The beta instrument testbed designed by Leardon Solutions includes a touch-screen electronic graphic interface in which different ePump parameters could be altered for testing. Duration of the pumping can be controlled, in addition to the specific ePump on the current can be adjusted to from 0-200mA. The eventual goal of the ePump is to have a reproducible pump rate that is controllable by adjusting the amount of current running through the electrodes, so testing was conducted using the beta instrument testbed in order to explore the relationship between current and flow rate.

The same testbeds and water displacement quantification as mentioned in other ePump experiments was used to evaluate pump rate. The original liquid electrolyte, 1M sodium sulfate, was used at 155µL (calculated to keep exposed surface area of electrodes constant for future comparison with experimental data of pumping with 150µL of the electrolyte inside a capsule) and directly pipetted into the ePump testbed's capsule chamber instead of encapsulation to ignore the issue of venting in capsules. Triplicates of tests using 50, 100, 15, and 200mA for 350

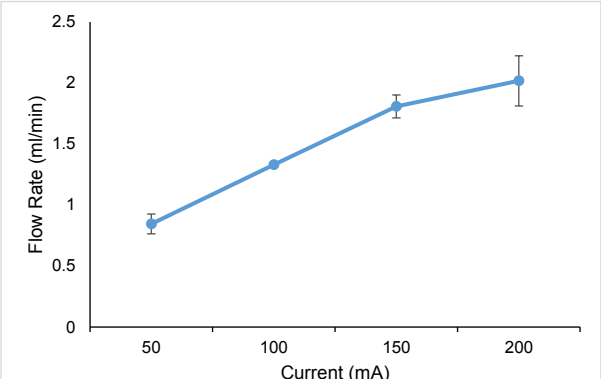

seconds of pumping were then conducted.

Figure 13 reflects a linear relationship between current and flow rate as expected: according to the trendline, an increase in 50mA of current corresponds to an increase in flow rate by 24μL/min. The upward trend of increasing current to increasing pump rate continues for 200mA, but the effect of the current increase is not at effective, likely due to limitations from the intrinsic resistance in the electrode-to-testbed interface. In fact, the greater deviation in pump rate for 200mA makes them almost comparable to pump rates from 150mA.

This characterization confirmed expectations for a linear relationship between current and pump rate, and similar trendlines can be obtained in the future to calculate the appropriate current setting corresponding to a target flow rate for a specific ePump. The flow rate at alpha's current setting of 100mA was well above the target ePump rate range of 1mL/min, so further confirmation that the linear trend applies even below 50mA should be conducted in order to achieve pump rates below 1mL/min. The additional parameter of loading conditions will also need to be factored in: testing has been using water displacement for quantification, but the ePump will eventually be used to pump sputum samples among other buffers in the cartridge. Having a more viscous liquid with different properties will likely affect the performance of the ePump, so this intersectionality will need to be explored and quantified in future progress.